Interferometric sizing of single-axis birefringent glass fibres

By

F. Onofri[(1)], A. Lenoble[(1)] , H. Bultynck[(2)], P-H. Guering[(2)], N. Marsault[(3)]

[(1)] UMR n°6595 IUSTI/CNRS-Université de Provence
Polytech'Marseille, Mechanical Engineering Department
Technopôle de Château-Gombert, 13453 Marseille Cedex 13, France
Email: Fabrice.Onofri@polytech.univ-mrs.fr
[(2)] Saint-Gobain Recherche, 93303 Aubervilliers Cedex, France
[(3)] Saint-Gobain Vetrotex International, 73000 Chambéry, France

1 ABSTRACT

This paper deals with the on-line sizing of small diameter glass fibres (i.e. $d<30\ \mu m$) produced for textiles and reinforcements applications.
A model to predict the basic light scattering properties of an infinite fibre is introduced. This model, based on the Lorenz-Mie Theory, take into account for various effects such as the high refractive index of *E-glass*, the fibre single-axis birefringence which is mechanically induced during the fibre forming process, the fibre refractive index dependence with size and temperature. A second model is introduced to predict the response of a phase Doppler interferometer to the on-line measurement of the fibre size.
Numerical results show that the influence of the refractive index dependence with size and tension, on the mean phase-diameter relationship (PDRS), is rather weak. Nevertheless, these effects have some influence on the resonance structure of the PDRS.
The principle of a numerical procedure, which allows determining the optical parameters leading to a minim error on the size measurements, is introduced. Four optimum optical arrangements have been identified. Two of them have been tested experimentally.
As first results, a satisfactory agreement have been found between: off-line measurements, obtained with a scanning electron microscope on fixed fibres, with on-line measurements (during the forming process), obtained with a integrated backward Phase Doppler Interferometer (PDI), a masse balance method and hydrodynamic considerations. The high temporal or spatial resolution of the two PDIs developed allow to study the stability of the drawing process regarding to various perturbations sources: gas bubbles in the glass melt composition, convective perturbations…

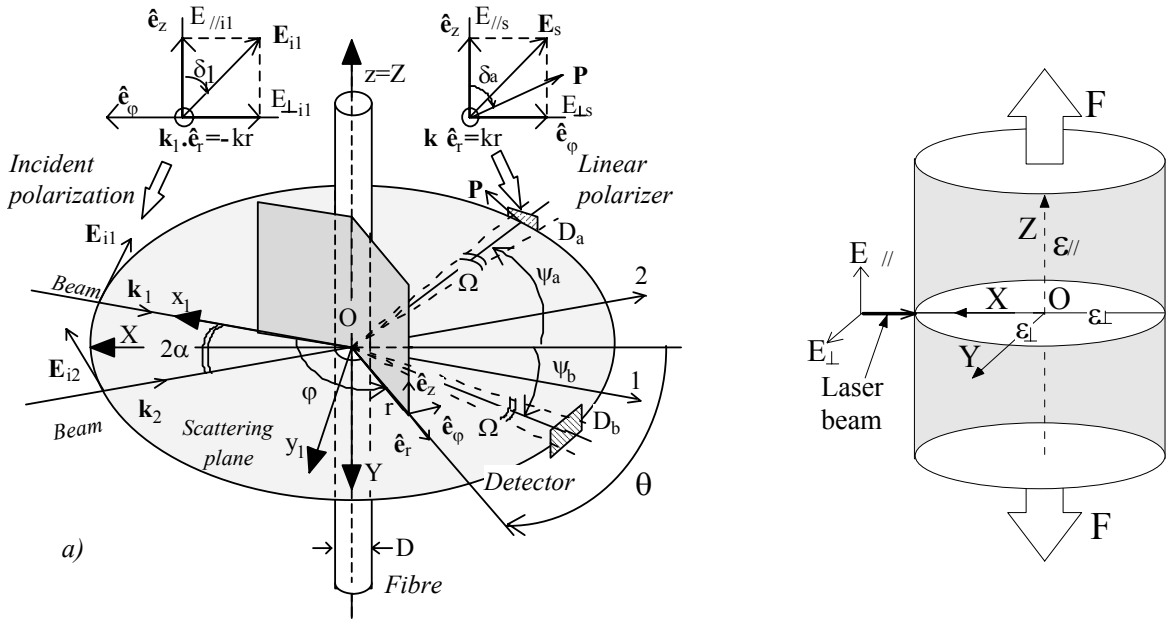

Fig. 1 a) Geometry for the scattering model and b) for a single-axis birefringent fibre

2 INTRODUCTION

The glass fibres used for textiles or for reinforcing plastic matrix are produced by a continuous forming process where a vertical jet is generated by a flow of molten glass through a cylindrical nozzle (e.g. Gupta, 1988). The jet is simultaneously cooled and attenuated under mechanical tension. The solidified jet is wound on a rotating wheel which provides the required tension. The forming process is clearly axisymetric. The jet, after a contraction factor of *250* to *500*, reaches a constant diameter *D* for a distance from the nozzle exceeding *15* to *20* times the nozzle diameter *(D_0#2mm)*. For continuous fibre forming and a given chemical melt glass composition, the fibre diameter is mainly controlled through the adjustment of the melt glass fiberizing temperature and the fibre take up velocity (imposed by the wheel rotation frequency). For commercial *E glass* fibres, typical values for the fiberizing temperature and the take up velocity are in the range *1230-1300°C* and *10-50m/s*. For a distance from the nozzle above *#250* times the nozzle diameter, the fibre temperature is only of few degrees above the ambient temperature.

In the manufacturing process several hundredth of fibres are produced at the same time to form a bundle (i.e. strand). The distribution of the diameter of the fibres plays an important role in the physical performance of the final product. So that, the ability to the monitor the characteristics of small fibres is important for viewpoint of both manufacturing efficiency and quality control. It is also suitable for the validation of basics models (e.g. Lenoble et al., 2002) on the stability of the drawing process in respect to various perturbations sources: heterogeneity of the glass melt composition and temperature, fluctuations in the take up velocity or in the hydrodynamics conditions of the drawing process (turbulence, radiative heat transfer...). So that there is actually a strong need for highly time resolved measurements of the size of the fibres during the forming process.

The measurement methods for the diameter of the fibres currently in use in the fibreglass industry are mainly off-line techniques: weighting techniques (the mean diameter is deduced from a mass balance and the measurement of the length of the sample), air permeability experiments or scanning electron microscopy. The two former techniques give only access to average quantities whereas the latter one gives detailed informations (shape, surface roughness and size) but at a very small scale, which limits its practical interest to study of the stability of the process to various temporal perturbations. On-line optical techniques such as diffraction (e.g. Lynch and Thomas, 1971) or micro-video imaging techniques (Gliksman, 1968) are mostly used for basic researches. Their resolution on the size of a single fibre is nevertheless limited (Gupta, 1988) particularly when considering that, due to the temperature and moisture environment of the forming process, the receiving optics cannot be positioned close to the fibre to be measured.

It has been shown recently (Mignon et al. 1996; Schaub et al., 1998) that, in the case of fibres with a circular cross-section and an isotropic material, the Phase Doppler interferometric (PDI) technique has the potential to provide in situ real-time measurement of the distribution of the diameter of fibres. Mignon et al. have described the light scattering properties of fibres using Geometric Optics, with a special emphasize on the influence on the size measurement of the fibres tilt angle compared to the plane of the laser beams. One limiting point in this earlier work is that, due to the simple scattering model used, there is no predictions of the resonance structure and of the other non-linearities of the phase-diameter relationship (PDRS). Schaub et al. have developed a more rigorous model, based on the Lorenz-Mie Theory (LMT), for the prediction of the PDI response to the sizing of infinite fibres with possible tilt angle. Various optical configurations for the design of a PDI system dedicated to the sizing of glass fibres are provided too. This work is nevertheless mainly dedicated to the sizing of fibres used for thermal insulation. So that this work does not take into account for some effects characteristic of the forming process of reinforcement fibres: the high refractive index of *E glass*, the mechanically induced birefringence of the fibres due to the high tension stress, the refractive index dependence of glass fibres with their size…

In this paper, a rigorous light scattering model and an optimization procedure taking into account all of the previously listed effects are introduced. Sections 2 and 3 presents the theoretical model developed to predict the basic light scattering properties of a single fibre and the model for the response of a PDI system to the sizing of an infinite birefringent cy fibre. Numerical results on the influence of various parameters on the PDI response are presented in section 4 as well as the optimization procedure developed to select the optical setups, which allows minimizing the error on the estimation of the fibre size. Section 4 presents the experimental setups and results carried out to validate the models developed. Section 5 is a conclusion including perspectives for future developments and improvements.

3 SCATTERING MODEL

3.1 Light scattering by an infinite right circular homogeneous cylinder

The fibre is considered as an infinite and homogeneous right circular cylinder with axis *Z* and diameter *D*, see Figure 1 a). A local Cartesian coordinate system *($Ox_1\ y_1\ z$)* is defined like the incident wave *i*, with wave vector $\mathbf{k_1}$, propagates along *(Ox_1)*, i.e. $\boldsymbol{k_1} = -k_1\boldsymbol{e_{x1}}$,. The incident wave is considered as a linearly polarized harmonic plane wave with pulsation ω_1 and wavelength λ. The electric field vector $\mathbf{E_1}$ of the incident wave can be decomposed into one component parallel, $E_{//}\mathbf{e}_z$, and one component perpendicular, $-E_{\perp}\mathbf{e}_{y1}$, to the plane *($x_1z$)*. The polarization angle of the incident wave will be referred as the angle δ_1 between the *z*-axis and the direction of the incident electric field vector $\mathbf{E_1}$. That is, we write the incident field as

$$\mathbf{E}_1 = \left(E_{//1}\cos\delta_1\mathbf{e}_z - E_{\perp 1}\sin\delta_1\mathbf{e}_y\right)\exp\left[i\left(-k_1x_1 - \omega_1 t\right)\right] \tag{1}$$

The laboratory coordinate system *(OXYZ),* with z =Z, is defined like the coordinate system (Ox_1y_1z) can be deduced by a rotation around the *z*-axis of the angle $-\alpha$.
A cylindrical coordinate system *($O\ r\varphi\ z$)* is introduced where the scattering angle φ is defined as the angle between the x_1-axis and the scattering direction $\mathbf{e_r}$. The field scattered by the fibre, subscript s, is the sum of two perpendicular components

$$\mathbf{E}_{s1} = E_{//s1}\mathbf{e}_z + E_{\perp s1}\mathbf{e}_\varphi \tag{2}$$

Under normal incidence (the light is only scattered in the plane *Z=0*) and in the far field, the asymptotic expressions for the amplitude of scattered field, in the scattering direction $\theta=\pi-\varphi$ and at a distance *r* from the fibre (with $kr >> 1$), reduce to (e.g. Bohren and Huffman, 1983):

$$\begin{pmatrix} E_{//s1} \\ E_{\perp s1} \end{pmatrix} = \exp\left[i\left(\frac{3\pi}{4} - k_1x_1\right)\right]\sqrt{\frac{2}{\pi kr}}\begin{pmatrix} T_1(\theta) & 0 \\ 0 & T_2(\theta) \end{pmatrix}\begin{pmatrix} E_{//1}\cos\delta_1 \\ E_{\perp 1}\sin\delta_1 \end{pmatrix}\exp\left[i\left(kr - \omega_1 t\right)\right] \tag{3}$$

The two terms $T_1(\theta)$ and $T_2(\theta)$ of the amplitude scattering matrix read as:

$$\begin{aligned} T_1(\theta) &= \sum_{-\infty}^{+\infty} b_{nI}\exp\left[-in\theta\right] = b_{0I} + 2\sum_{n=1}^{+\infty} b_{nI}\cos\left(n\theta\right) \\ T_2(\theta) &= \sum_{-\infty}^{+\infty} a_{nII}\exp\left[-in\theta\right] = a_{0II} + 2\sum_{n=1}^{+\infty} a_{nII}\cos\left(n\theta\right) \end{aligned} \tag{4}$$

Where b_{nI} and a_{nII} are the external scattering coefficients for an infinite and homogeneous right circular cylinder and for the incident beam components $\mathbf{E}_{\|1}$ and $\mathbf{E}_{\perp 1}$ respectively. These functions, which encounter for the particle properties (diameter and refractive index), are complexes functions which requires calculations of Hankel and Bessel functions of the first kind with their derivatives.

It can be useful to study the degree of linear polarization of the light scattered by the fibre, and this particularly for the diagnosis of birefringent fibres. To do so, a part of the light that is scattered by the fibre is collected by a detector composed of a collimating lens, passed through a linear polarizer, and finally focused onto a photo detector. In Figure 1 a) and for detector D_a, the polarizer axis *P* makes an angle δ_a with $\mathbf{e}_z$. Finally, the scattered field after the linear polarizer reads as:

$$\begin{pmatrix} E_{//s1} \\ E_{\perp s1} \end{pmatrix}_P = \begin{pmatrix} \cos^2\delta_a & \sin\delta_a\cos\delta_a \\ \sin\delta_a\cos\delta_a & \sin^2\delta_a \end{pmatrix}\begin{pmatrix} E_{//s1} \\ E_{\perp s1} \end{pmatrix} \tag{5}$$

The scattered energy at position *($r\theta\ z$)*, over the time duration $1/\omega_1$, may be calculated with the help of the Poynting's vector:

$$\left\langle \mathbf{S_s} \right\rangle_{1/\omega_1} = \frac{1}{2}\mathrm{Re}\left\{ \mathbf{E_s} \times \mathbf{H_s^*} \right\} \tag{6}$$

In a free homogeneous and non-magnetic medium with magnetic permeability μ_0, the Poynting's vector reduces to

$$\left\langle \mathbf{S_s} \right\rangle_{1/\omega_1} = \frac{1}{2\omega_1\mu_0}\mathrm{Re}\left\{ \mathbf{E_s} \times \left(\mathbf{k} \times \mathbf{E_s} \right)^* \right\} = \frac{\mathbf{k}}{2\omega_1\mu_0}\mathrm{E_s}\mathrm{E_s^*} \tag{7}$$

3.2 Refractive index dependence with drawing stress

During the forming process, the fibre is submitted to a high mechanical tension, *F*. This tension or drawing stress is typically of *0.497* and *0.36 grams* for fibres of *5* and *10 μm* respectively, i.e. a tension of *632* and *115* kilograms per square centimetre. Under such constraint, the fibre material (glass) may be birefringent. It is expected to be single-axis (optical axis along the fibre axis *Z*) due to the symmetry of the drawing process, see Figure 1 b). The fibre birefringence, which is expected to vanishes when it is cut, but not completely (e.g. Gupta, 1988), has to be taken into account to predict the light scattering properties of the fibre during the process. Following the previous remarks, the fibre material permittivity tensor is like

$$\begin{pmatrix} D_X \\ D_Y \\ D_Z \end{pmatrix} = \begin{pmatrix} \varepsilon_\perp & 0 & 0 \\ 0 & \varepsilon_\perp & 0 \\ 0 & 0 & \varepsilon_\mathrm{P} \end{pmatrix} \begin{pmatrix} E_X \\ E_Y \\ E_Z \end{pmatrix} \tag{8}$$

Neglecting absorption of glass in the visible range, the fibre extraordinary refractive index, $m_{//}$, and the fibre ordinary refractive index, $m_\perp$, can be related to the electrical permittivity constants with

$$m_\perp = \sqrt{\frac{\mu\varepsilon_\perp}{\mu_0\varepsilon_0}},\ m_{//} = \sqrt{\frac{\mu\varepsilon_{//}}{\mu_0\varepsilon_0}} \tag{9}$$

Assuming that the fibre birefringence $(m_{//} - m_\perp)$ is proportional to the tension *F* apply to the fibre we found that

$$m_{//} - m_\perp = -m_\perp \sigma\left(T_0\right)\left(\frac{1.29\ 10^4 F}{D^2} \right) \tag{10}$$

Where *F* is the drawing tension applied to the fibre in grams, σ the optical stress coefficient of the fibre material and *D* the diameter of the fibre in microns. σ depends on the forming process conditions and mainly on the nozzle temperature, T_0, which has a strong influence on the glass melt viscosity. For the drawing of *E glass*, with a nozzle temperature of T_0=*1200°C*, the optical stress coefficient is about $\sigma \# 6\ 10^{-7}\ MPa^{-1}$. By using Eq. (10) we found that the difference between the two refractive index is of $2.4\ 10^{-4}$ and $4.3\ 10^{-5}$ for a fibre of *5 μm* and *10 μm*.

From Eqs. (3) it appears that the scattered field component, $E_{//s}$, depends only on the external scattering coefficients b_{nI} and, $E_{\perp s}$, depends only on the external scattering coefficients a_{nII}. In fact, the scattering coefficients depends themselves on the laser wavelength, the fibre size and refractive index (relative to the external medium refractive index). So that, to predict the scattered field by a single-axis birefringent fibre, we only have to use Eq. (3) and Eq. (5) (if a linear polarizer is used) with $b_{nI}\left(\lambda, D, m = m_\mathrm{P}\right)$ and $a_{nII}\left(\lambda, D, m = m_\perp\right)$.

3.3 Refractive index dependence with diameter and temperature

There is several reports in the literature (e.g. Gupta, 1988, Corpus and Gupta, 1993) about the fact that the mechanical and optical properties of the fibres depend not only on the chemical composition of the initial glass melt but also on their forming conditions. Corpus and Gupta have developed a simple model to predict the refractive index dependence with the fibre diameter (Corpus and Gupta, 1993). It is based on the three following considerations: *ii) m* depends on the fictive temperature of a glass T_f, *iii)* T_f of a glass depends on its cooling rate *q*, *i)* the maximum *q* experienced by a fibre is inversely proportional to the square of *D*. Note that Corpus and Gupta have found a good agreement between their model and experimental data obtained for a soda-lime-silica melt of *NBS-170* composition.

From this work, we have derived the following analytical relation for the dependence of the refractive index of the fibre with its diameter (i.e. Thermal history):

$$m(D)_T = \sqrt{\frac{\beta_T\left(\theta_T+2\right)\ln(D)+\alpha_T(\theta_T+2)-1}{\beta_T\left(\theta_T-1\right)\ln(D)+\alpha_T(\theta_T-1)-1}} \tag{11}$$

To estimate the coefficients α_T, β_T and θ_T, for *E-glass* , we have used the experimental results from Clementin-de-Leusse, 2000. A non-linear curve fitting procedure was used to fit the experimental data points with Eq. (11), so that we have found α_T *=119.68047*, β_T *= -82.49331* and θ_T*=3.10733*.

4 MODEL FOR THE PHASE DOPPLER RESPONSE

To modelize the response of a PDA system when measuring a single-axis birefringent fibre under normal incidence, one has to compute the interference field pattern produced onto the detector aperture when the fibre is located at the crossing of two *TM00* laser beams *1* and *2*. It is assumed here that the waist of each beam is located at the beams crossing and its size is far superior to the diameter of the fibre. These conditions being fulfilled we can use the previous results obtain for incident plane waves (Gouesbet et al., 1998).

The fibre is assumed to have only small displacements in the *(OXY)* plane. This condition is necessary to be under the remote detector approximation (i.e. small displacements of the fibre do not change the scattering angles). It may have a high velocity along the *Z*-axis (as usually in the drawing process). To take into account for beam 2, we introduce, as previously done form beam *1*, an additional local Cartesian coordinate system *(Ox_2 y_2 z)*. Each beam has a given polarization angle, δ_1 and δ_2, and a given pulsation ω_1 and ω_2. Note that in the principle of the PDI technique, the two laser beams are frequency shifted each other with Bragg's cells or with a rotating transmission grating (e.g. Durst et al., 1981). Among other features, this allows to get frequency-modulated signals whatever the particle is fixed in the probe volume.

We now consider a point detector D_a with a polarizer angle δ_a, located in the OXYZ plane with (Z=0), distant of *r* from the fibre and positioned at elevation angle ψ_a, see figure 1 a), In this configuration detector D_a is located at the following scattering angles: for beam *1*, $\theta_1=\psi_a-\alpha$ and for beam *2:* $\theta_2=\psi_a+\alpha$.
Using Eq. (2) the scattered field collected by the detector reads as,

$$\mathbf{E}_s\left(\psi_a\right)=\left[E_{//s1}\left(\psi_a-\alpha\right)+E_{//s2}\left(\psi_a+\alpha\right)\right]\mathbf{e}_z+\left[E_{\perp s1}\left(\psi_a-\alpha\right)+E_{\perp s2}\left(\psi_a+\alpha\right)\right]\mathbf{e}_\varphi \tag{12}$$

For the case where $\omega_1/\omega_2 \sim 1$, the Poynting vector reduces to:

$$\mathbf{S}_s=\frac{\mathbf{k}}{2\mu_0\omega}\left[\left|E_{//s1}\right|^2+\left|E_{//s2}\right|^2+\left|E_{\perp s1}\right|^2+\left|E_{\perp s2}\right|^2+2\,\mathrm{Re}\left\{E_{//s1}E_{//s2}^*+E_{\perp s1}E_{\perp s2}^*\right\}\right] \tag{13}$$

the previous expression can be reformulated in the more convenient form:

$$\mathbf{S}_s=\frac{\mathbf{k}}{2\mu_0\omega}\left(G+\mathrm{Re}\left\{H\exp\left[-i\omega_D(t)\right]\right\}\right) \tag{14}$$

with,

$$G=\left|E_{//s1}\right|^2+\left|E_{//s2}\right|^2+\left|E_{\perp s1}\right|^2+\left|E_{\perp s2}\right|^2 \tag{15}$$

$$H=2\left(E_{//s1}E_{//s2}^*+E_{\perp s1}E_{\perp s2}^*\right) \tag{16}$$

$$\omega_D=\left(\mathbf{k}_1-\mathbf{k}_2\right)\cdot\mathbf{r}+\omega_s=-2V_Y\left(t\right)\frac{\sin\alpha}{\lambda}+\omega_s \tag{17}$$

In Eqs. (15) and (16) expressions for the scattered field components must be replaced by their proper expressions deduced from Eqs. (3) and (5) with, for instance, for beam *1* and detector D_a:

$$E_{//s1} = \exp\left[i\left(\frac{3\pi}{4} - k_1 x_1\right)\right]\sqrt{\frac{2}{\pi kr}}\left[\cos^2\delta_a T_1\left(\psi_a - \alpha\right)E_{P1}\cos\delta_1 + \sin\delta_a\cos\delta_a T_2\left(\psi_a - \alpha\right)E_{\perp 1}\sin\delta_1\right]\exp\left[i\left(kr - \omega_1 t\right)\right]$$
$$E_{\perp s1} = \exp\left[i\left(\frac{3\pi}{4} - k_1 x_1\right)\right]\sqrt{\frac{2}{\pi kr}}\left[\sin\delta_a\cos\delta_a T_1\left(\psi_a - \alpha\right)E_{P1}\cos\delta_1 + \sin^2\delta_a T_2\left(\psi_a - \alpha\right)E_{\perp 1}\sin\delta_1\right]\exp\left[i\left(kr - \omega_1 t\right)\right] \quad (18)$$

In Eq. (17) the scalar product $(\boldsymbol{k_1}-\boldsymbol{k_2})\boldsymbol{.r}$ has been reformulated in a time depend form by considering, following the so-called fringes model (e.g. Durst et al., 1981; Onofri et al., 2002), that there exit fringes in the probe volume with a fringe spacing, $i_f = \lambda/(2\sin\alpha)$. When the fibre moves slightly in the *(OXY)* plane the previous term depends on the fibre velocity component along the *Y*-axis, $V_y(t)$. This term is responsible for a frequency shift of the collected signal. Classically, the term ω_D is the so-called heterodyne Doppler frequency which depends on the particle velocity component $V_y(t)$ and on the frequency shift between the two beams $\omega_s=(\omega_1-\omega_2)/2>0$. During the forming process, any fluctuation of the position of the fibre in respect to the *Y*-axis could be detected from the fluctuation of the frequency, ω_D.

For a physical detector, Eq. (14) has to be integrated over its receiving aperture Ω. Under normal illumination, the integrating angle reduces to $[\psi_a-\Omega/2,\ \psi_a+\Omega/2]$. Thus, assuming a detector with a linear aperture and with a linear response (electrical signal proportional to the intensity of the light collected) the electrical signal output from this detector is

$$I(t) = \frac{k}{2\mu_0\omega}\int_{\Omega}\left|S_s(t)\right|d\psi \quad (19)$$

Using Eq. (14) the previous expression can be reformulated in the following form (Naqwi and Durst, 1993):

$$I(t) = \frac{k}{2\mu_0\omega}\left(\left\langle G\right\rangle_{\Omega} + 2\sqrt{\left\langle H_i\right\rangle_{\psi}^2 + \left\langle H_r\right\rangle_{\psi}^2}\cos\left[\tan^{-1}\left(\left\langle H_i\right\rangle_{\psi}/\left\langle H_i\right\rangle_{\psi}\right) - \omega_D t\right]\right) \quad (20)$$

Where the terms into brackets mean: integrated quantities over the detector-receiving aperture of the functions introduced in Eqs. (15) and (16), with

$$\left\langle G\right\rangle_{\Omega} = \int_{\Omega} G\,d\psi \qquad \left\langle H_r\right\rangle_{\Omega} = \int_{\Omega}\mathrm{Re}\left\{H\right\}d\psi \qquad \left\langle H_i\right\rangle_{\Omega} = \int_{\Omega}\mathrm{Im}\left\{H\right\}d\psi \quad (21)$$

We now introduce the mean pulsation $\omega=(\omega_1+\omega_2)/2$ and the new quantities $P,\ V,\phi$, usually known as the Doppler signal pedestal, visibility and phase respectively, with

$$\begin{aligned} P &= k\left\langle G\right\rangle_{\Omega}/\left(2\mu_0\omega\right) \\ V &= 2\sqrt{\left\langle H_i\right\rangle_{\Omega}^2 + \left\langle H_r\right\rangle_{\Omega}^2}/\left\langle G\right\rangle_{\Omega} \\ \phi &= \tan^{-1}\left(\left\langle H_i\right\rangle_{\Omega}/\left\langle H_i\right\rangle_{\Omega}\right) \end{aligned} \quad (22)$$

Finally, Eq. (20) can be reformulated to obtain the equation of a phase Doppler signal:

$$I(t) = P\left[1 + V\cos\left(\omega_D t + \phi\right)\right] \quad (23)$$

The phase ϕ in Eq. (23) is an absolute phase, which depends, in the remote detector approximation and for plane wave illumination, only on the optical setup and the properties of the fibre. As an absolute phase, it cannot be measured directly. So that, in the principle of the PDI technique, two detectors D_a and D_b or more (see also Onofri et al., 2002) are used to measure the phase difference between the two Doppler signals. From the two detectors, subscripts *a* and *b*, positioned at elevation angles ψ_a and ψ_b, we get two Doppler signals:

$$S_a(t) = P_a\left[1 + V_a\cos\left(\omega_D t + \phi_a\right)\right] \qquad S_b(t) = P_b\left[1 + V_b\cos\left(\omega_D t + \phi_b\right)\right] \quad (24)$$

The phase difference between $S_a(t)$ and $S_b(t)$, i.e. $\Delta\phi_{ab}=\phi_a-\phi_b$, can be, for instance, measured with the help of the cross spectral density function. The dependence of $\Delta\phi_{ab}$ with the diameter of the fibre, $\Delta\phi_{ab}=f(D)$, is usually referred as the phase-diameter relationship (PDRS). Note that in the principle of the PDI technique the size of the measured particle (sphere or fibre in the present case) is deduced from the measurement of the phase-difference $\Delta\phi_{ab}$ and from the knowledge of the PDRS.

The validation of the previous models was performed in three ways. First, we have compared our predictions with the predictions of a code devoted to spherical particles (Naqwi and Durst, 1993; Onofri et al., 1995). Second, we have compared our results with the results found in the literature for homogeneous fibres with a lower refractive index: based on Geometrical optics (Mignon et al., 1996) and on the Lorenz-Mie theory (Schaub et al., 1998). Note that a perfect agreement has been found with both results. Third, we have made comparisons with experimental data, as it will be detailed in section 5.

What we want to emphasize here is some of the discrepancies observed for the PDRS obtained for fibres and spheres. In figure 3 are presented the PDRSs for cylindrical and spherical particles within the size range *5-30 μm*. These calculations have been done for the optical arrangements (A) and (D) (see in Table 1) with in both cases: $\Omega/2=3.13°$ and $\alpha=0.885°$; (A): $\psi_a=-\psi_b=70°$; (D): $\psi_a=-162.7°$, $\psi_b=+166.7°$.
For arrangement (A), where the detectors are located in the forward region, there are only minor differences between the PDRSs. The only noticeable difference leads in a small phase-shift of the resonance structure. For arrangement (D), where the detectors are located in the near-backward region, there are significant differences, i.e. in the mean slope of the PDRSs and in the amplitude and phase of the resonance structure. So predictions of phase Doppler codes devoted to spheres should be carefully used when they are used to predict the Doppler signal properties for fibres.

5 OPTIMIZING PROCEDURE AND NUMERICAL RESULTS

5.1 Optimizing procedure

The objective of the numerical optimization of the optical setup of a PDI system consists in two key points: *i)* the reduction of the oscillatory behaviour of the PDRS, to ensure a higher accuracy on the measurement of the fibre size; *ii)* the reduction of the bulky design of the optical setup to fulfil constraint imposed by the industry environment. This optimization is clearly a multi-parameters study as the phase difference $\Delta\phi_{ab}$, as well as the signal pedestal and visibility depend of various factors: the optical parameters λ, δ_1, δ_2, α, ψ_a, ψ_b, Ω, δ_a and δ_b and the properties of the fibre (D, $m_{/\!/}(composition,F,D,T_0)$ and $m_{\perp}(composition,F,D,T_0)$.
Obviously, not all these parameters are of the same importance, so we need to define a criterion to quantify the relative importance of each of theses parameters. There are many ways to do so. In the present work, we have used the following procedure:

- The phase Doppler LMT based code is used to compute the theoretical PDRSs, $\Delta\phi_{ab\text{-}LMT}=f(D)$, for the set of parameters under study and for a fibre within the size range $D=5\text{-}30\ \mu m$;
- A least square algorithm is used to find the slope b and ordinate a of the linear regression, $\Delta\phi_{ab\text{-}Lin}=a+bD$, which better fits the previous PDRSs;
- The deviation from linearity as well as the amplitude of the resonance structure of the theoretical PDRS can be determined by calculating the following standard deviation coefficient $\sigma_{ab\text{-}\phi}=f(\Delta\phi_{ab\text{-}LMT}-\Delta\phi_{ab\text{-}Lin})$;
- Finally, this standard deviation may be used to estimate the mean error on the size of the fibre when the resonance structure and other nonlinearities are neglected, $\sigma_{ab\text{-}D}=\sigma_{ab\text{-}\phi}/b$.

5.2 Examples of numerical results

The influence of the fibre refractive index dependence with its size can be estimated from figure 5. In this figure the PDRS is shown when Eq. (11) is used or not (constant refractive index, m=1.555). Note that Eq. (11) introduces a change in the refractive index from 1.5407 to 1.5553 for a fibre in the size range 5-25 μm (see the subfigure in the bottom left corner of figure 5).
Whatever the change in the refractive index is rather important it has no significant influence on the PDRS except in a small shift of the resonance structure and this mainly for small diameters (see top left corner of figure 5). This last

remark can be simply explain by the shape of the refractive index dependence with the size, which sharply increases for sizes up to 8-10 µm and then decreases for larger sizes. The relative weak influence of this refractive index dependence, over all the PDRS, may be explained by the small evolution of the refractive index of the fibre compared to its size. The calculations presented in figures 5 and 6 corresponds to the experimental parameters of the near-backward interferometer **Fibs** (see figure 7) of type (D), with $\Omega/2=4.89°$, $\alpha=1.094°$; $\psi_a=-166.7°$ and $\psi_b=+162.5°$.

The influence of the fibre axial stress on the PDRS can be estimated from figure 6. In this figure is plotted the difference between: the PDRS when Eq. (10) is used (fibre under tension, i.e. during the forming process) and the PDRS when Eq. (10) is not used (fibre cut, i.e. off-line measurements). These calculations have been done for the size range *5-6 µm*.
Some peaks can be observed in this figure they correspond to sharp resonances, which occur for different refractive indices (i.e. axial stress in the present case). If one neglects these sharp resonances, the mean standard deviation between the two relationships is about 0.55°. Knowing the mean slop of the total PDRS, it follows that the axial-stress induces an error on the fibre diameter of less than *0.04 µm*. Obviously, the error may become drastic when a sharp resonance is measured.

Figure 4 presents an iso-level map of the estimated mean size error, for fibres in the size range *5-30 µm*, versus the elevation angle of both detectors. For these calculations, we used the optical parameters of table 1, without polarizer as all the results presented here. The Top left corner corresponds to incident beams with polarization perpendicular to the scattering plane *(OXY)* and the bottom right corner corresponds to incident beams with polarization parallel to the scattering plane. Four zones or optical arrangements (A), (B), (C) and (D), corresponding to a minimum size error, can be identified in this map. Note that here, for drawing considerations, the estimated error is set negative when the slope of the PDRS is negative (it corresponds to a dominant reflective scattering process) and it is set positive when the corresponding slope is positive (it corresponds dominant refractive process scattering process).

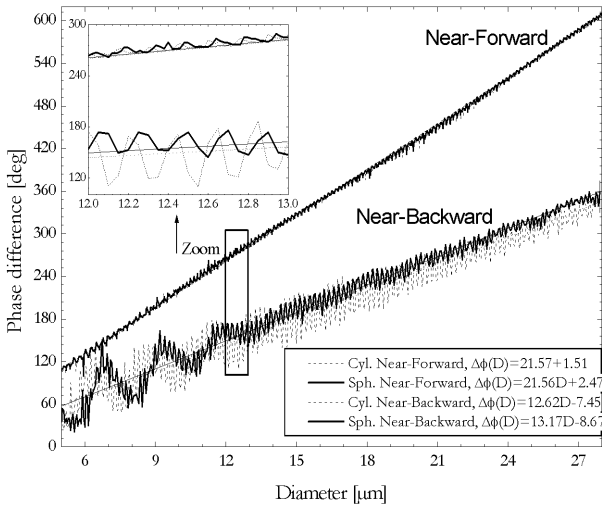

Fig. 3 Comparison between the phase-diameter relationships predicted for optical arrangements of types (A) and (D) when the scattering particle is a cylinder or a sphere.

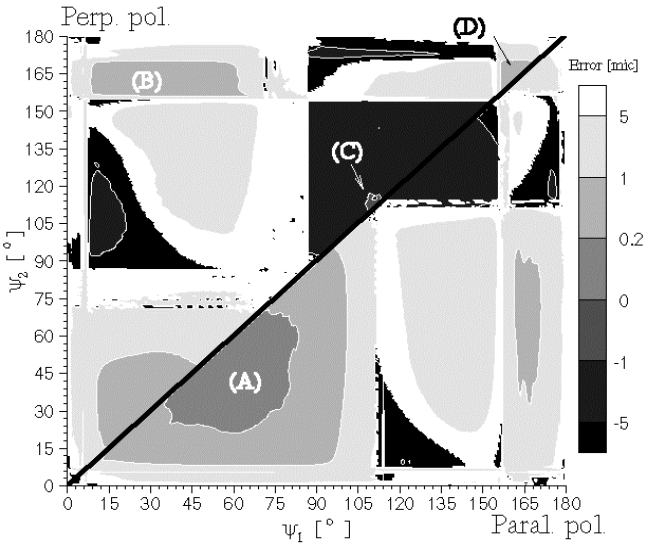

Fig. 4 Iso-level map of the estimated error (standard deviation from linearity) versus the position of the two detectors. Top left corner: for incident beams with polarization perpendicular to the scattering plane. Bottom right corner: for incident beams with polarization parallel to the scattering plane.

- Zone (A), for parallel polarization, corresponds to an optical arrangement where the two detectors are located in the forward in a plus or less symmetrical way in respect to the optical axis *(OX)*. In this region, the dominant scattering process is a refraction process. In table 1 the parameters of this configuration are details. It corresponds to a minimum standard deviation on the size of the fibre of #0.12 µm.

- Zone (B), for perpendicular polarization, corresponds to an optical arrangement where the two detectors are on the same side of the optical axis. One is located in the forward region (the dominant scattering process is single refraction) and the other one is located in the so-called rainbows region (refracted rays with one or two internal reflection). From

our simulation, it appears that this unusual optical arrangement provides a good accuracy on the fibre size (see table 1). Nevertheless, its bulky geometry may be a major limitation for applications in industry.

- Zone (C), for perpendicular polarization, corresponds to an optical arrangement where the two detectors are on both sides ways of the optical axis and more precisely in the so-called Alexander dark band (the dominant scattering process is reflection). This scattering mode is usually considered as the less sensible to any change in the fibre material homogeneity. Nevertheless, this arrangement provides the worst accuracy on the fibre size compared to other geometries.

- Zone (D), for perpendicular polarization, corresponds to an optical arrangement where the two detectors are both in the rainbows region. This optical arrangement is clearly the more compact one. It provides a rather an acceptable accuracy on the size of the fibre (standard deviation: #0.34).

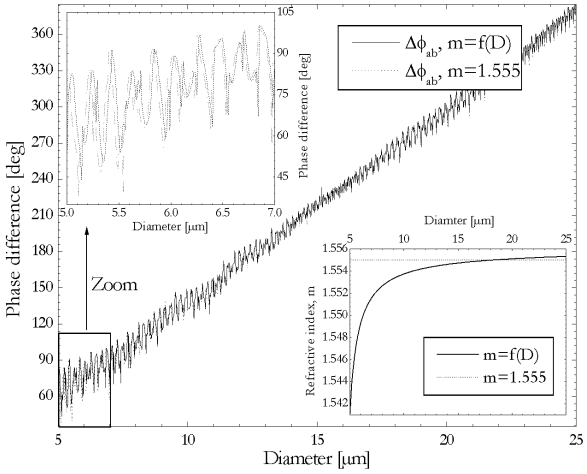

Fig. 5 Evolution of the phase-diameter relationship when the refractive index dependence with the fibre size is taken into account or not.

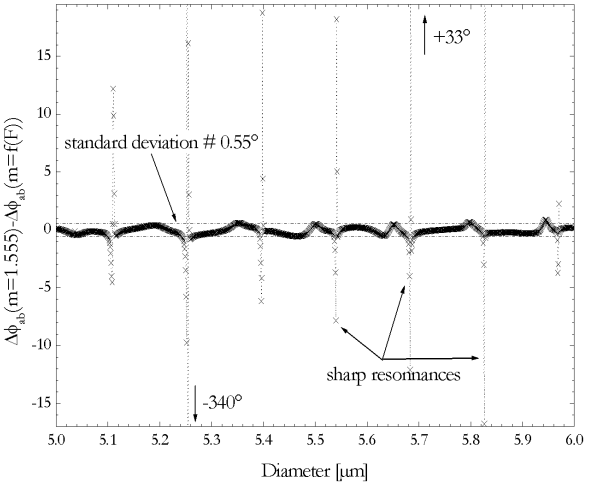

Fig. 6 Evolution of the difference between the phase-diameter relationships calculated for the fibre under tension (birefringence, during the process) and without tension (homogeneous material, fibre cut).

6 EXPERIMENTAL SETUP AND RESULTS

6.1 Experimental setup

Only the geometries (A) and (D) were tested experimentally. For this purpose, we built two interferometers. Fig 7 shows the backward system, (D). They were both build with the same optical and hardware components.
The output of *2.5 mW* linearly polarized Helium-Neon laser is focus onto a rotating transmission diffraction gratings. The diffracted beams are collimated with a spherical lens and a beam stop is use to stop all the diffracted beams with order different of order ± 1. The two out coming beams are collimated and next, focussed by a transmission lens with focal length *450 mm.* The probe volume diameter is of *#300 µm*. The use of a half-wave retardation plate and the selection of the diffraction gratings rotating velocity allow controlling the laser beams polarization and beams frequency shift ω_s. The light scattered by the fibre, when it is in the prove volume, is collected by two receiving optics composed with a set of two achromatic lenses, with a collection angle *Ω/2=4.9°* and a focal length of *450 mm*. Then the collected light is focused onto two multimode polymer fibres. Two pre-amplified Avalanche Photo Diodes (APDs) with bandwidth (0.1kHz-10MhZ) are used for the conversion of optical signals in electrical signals. All theses components are included in the head of the interferometer (shown in figure 7).
The electrical output of the two APDs is digitized with a data acquisition board. A PC is used for the signal processing. A data acquisition and a processing software, using a sliding Cross Spectral Density (CSD) function algorithm, was developed to measure the phase difference between the raw Doppler times series (which looks like two phase-shifted infinite sinusoidal time series). For the typical experimental results presented bellow the diffraction gratings velocity was set to get a frequency shift of ω_s *# 250 kHz*. With a sampling acquisition rate of *1 MHz*, and calculation windows of *32* samples for the CSD calculations, this ensures *38500* measurements per second (i.e. a longitudinal resolution of *1.3* millimetre) for a fibre take up velocity of *50 m/s*.

Experiments were carried out on a laboratory scale single-fibre drawing bench developed by Saint-Gobain Vetrotex Int. as well as on fixed fibres.

6.2 Example of experimental results

Fig. 8 shows a comparison between the mean size of the fibre, measured during the drawing process under stationary conditions, with, the near-backward interferometer *Fibs* over 9 minutes (i.e. fibre length: *4-24 km*); results from a mass balance method and from hydrodynamic considerations (based on the mass flow rate and the bulb temperature); versus, the size measured with a Scanning Electron Microscope (SEM) for several samples of fibres.
All the measurements are in rather good agreement. Some of the discrepancies observed can be explain with the following arguments: SEM measurements were performed on a single fibre which size may be not representative of the mean size of the whole fibres sample; *ii)* we were not totally confident in the calibration of the SEM used for this experiment (in Fig. 8, for large fibres, the SEM seems to over estimate the fibre size compared to the 3 other techniques); *iii)* we have neglected the resonance structure of the PDRS; *iv)* there is some uncertainties in the glass density (i.e. refractive index too); *v)* the measurement of the bulb temperature with an optical pyrometer is subject to errors which have a strong influence on the estimation of the glass viscosity and then on the predictions of the hydrodynamic model.

Fig. 9 shows the evolution of the fibre diameter, measured during the drawing process with system (A), when the bulb is submitted to a short convective perturbation (one blows on the bulb). Strong fluctuations of the fibre size are observed. After few seconds (i.e. more than *160 m*) the fibre returns to its nominal size *#8.3 µm*, without breaking.

Fig. 10 presents the response of system (A) when a hollow fibre is measured (gas bubbles were generated in the glass melt composition). Fibres with a gas core induce sharp oscillations of the measured phase difference, which can not be, at the moment, related to the fibre outer diameter. Nevertheless, these sharp oscillations are a good indicator of the presence of gas bubbles in the glass melt composition, which is already important information. In Figure 10, the fibre initial and final diameter is about *8.2 µm (A, D)*. From the time duration of the sharp resonances we can estimate the length of the hollow fibre: *L#2 m* for (B) and *L#0.6 m* for (D).

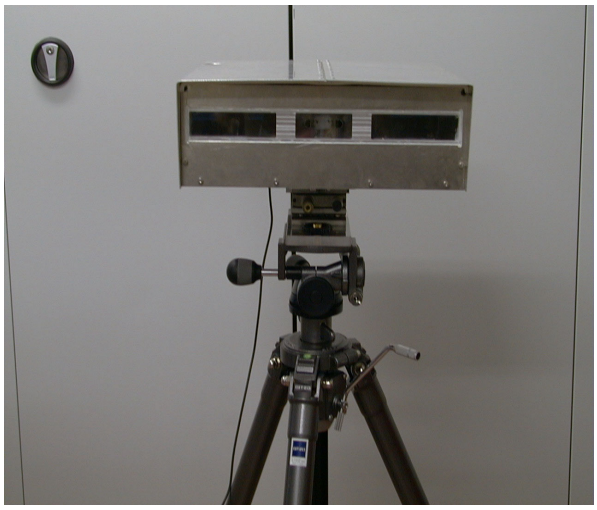

Fig. 7: ***Fibs:*** *near-backward interferometer.*

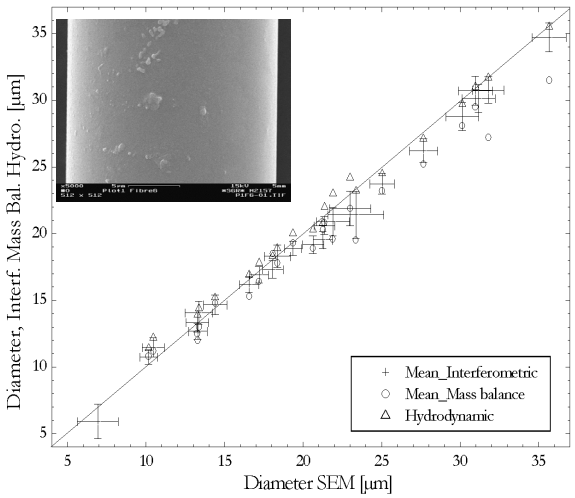

Fig. 8: Comparison between the fibre mean diameter measured during the forming process with:Fibs, a mass balance method, hydrodynamic calculations; versus off-line SEM measurements on a single fibre.

7 CONCLUSION

A model to predict the basic light scattering properties of an infinite fibre is presented. This model, based on the Lorenz-Mie theory, take into account for various effects such as the high refractive index of *E-glass*, the fibre single-axis birefringence induce by the tension applied during the forming process, the fibre refractive index dependence with its size due to the differences in the cooling rates. A second model is introduced to predict the response of a Phase Doppler laser interferometer to the on-line measurement of the size of a single-fibre. Results show that the influence of the refractive index dependence with size and tension, on the mean phase-diameter relationship (PDRS), is rather weak. Nevertheless, these effects have a significant influence on the resonance structure of the PDRS. It is expected

that birefringence could have a higher influence when measuring, for instance, polymer fibres which have a higher optical stress coefficient. The optimization procedure has shown that there exist four optical arrangements leading to a minimum error on the fibre size. Two of them have been tested experimentally. As first results, a satisfactory agreement has been found between experimental and numerical results. The high temporal (i.e. spatial) resolution of the two PDI developed allows to study the stability of the drawing process regarding to various perturbations sources: gas bubbles in the glass melt composition, convective perturbations… Work is under way to the use the PDRS to increase significantly the resolution on the measurement of the size of the fibre or to allow the measurement of the fibre tension.

Parameters		Arrangements			
		(A)	(B)	(C)	(D)
λ	[µm]	0.632	0.6328	0.6328	0.6328
m		1.555	1.555	1.555	1.555
$\alpha/2$	[deg]	0.9	0.9	0.9	0.9
$\Omega/2$	[deg]	6.0	6.0	6.0	6.0
Polar. (scat. plane)		//	$\perp$	$\perp$	$\perp$
ψ_a	[deg]	+63.0	+26.0	+110.	+161.
ψ_b	[deg]	-55.0	+162.5	-113.5	-165.0
σ_D	[µm]	0.12	0.31	-0.96	0.34
b	[µm/deg]	16.08	12.06	-10.67	13.42

Table 1. Optical parameters of the four optical setups identified from the optimization procedure, size range: 5-30 µm.

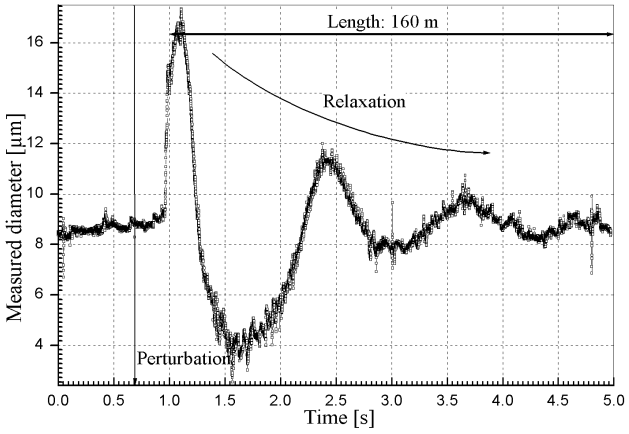

Fig. 9 Evolution of the fibre diameter when the bulb is submitted to a convective perturbation.

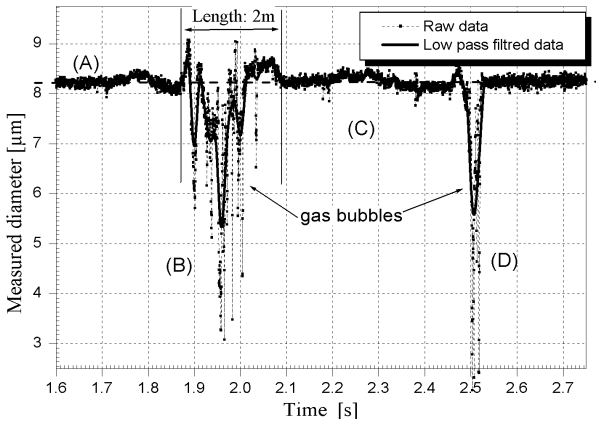

Fig. 10 Evolution of the fibre diameter when gas bubbles are included in the glass melt composition.

8

9 ACKNOWLEDGMENTS

The authors are grateful to ADEME (French Agency for the Environment and Energy Resources) for providing partial financial support for this work.

10 REFERENCES

Bohren C.F., Huffman D.R. (1983), Absorption and Scattering of Light by Small Particles, (John Wiley \& Sons, NY).

Clementin-de-Leusse C. (2000), "Etude de fibres de verre E. Caractérisation expérimentale par spectrométrie de Brillouin et test de modèle de fribrage", PhD thesis, Univ. de Monpellier II, France.

Corpus J.M. and Gupta P.K. (1993), "Diameter dependence of the refractive index of melt-drawn glass fibres", J. Am. Ceram. Soc. 76, 1390-392.

Durst F., Melling A. and Whitelaw J.H. (1981), Principles and Practice of Laser-Doppler Anemometry, (Academic Press, London).

Gouesbet G. , Gréhan G. and Ren K. F. (1998), "Rigorous justification of the cylindrical localized approximation tospeedup computations in the generalized Lorenz-Mie theory for cylinders", J. Opt. Soc. Am. A 15 , 511 - 523.

Gliksman L.R. (1968), "The Dynamics of a Heated Free jet of Variable Viscosity Liquid at Low Reynolds Numbers", J. of Basic Eng. 90, 343-354.

Gupta G. (1998), Fibres Reinforcements for composite materials, Chapt. 2 (A.R. Bunsell, edited by ELSEVIER).

Lenoble A., Onofri F. and Radev S., "Modélisation physique du procédé de fibrage des fibres de renforcement", Congrés français de thermique, SFT 2002, Vittel, 3 - 6 juin 2002

Lynch L.J. and Thomas N. (1971), "Optical Diffraction Profiles of Single Fibres", Textile Research J., 41, 568-72.

Mignon H., Gréhan G., Gouesbet G., Xu T-H. and Tropea C. (1996), "Measurement of cylindrical

particles with phase Doppler anemometry", Appl. Opt. 35, 5180-5190.

Naqwi A. and Durst F. (1993), "Analysis of the light scattering interferometric devices for the in-line diagnosis of moving particles", Appl. Opt. 32, p4003 - 4018.

Naqwi A., Hartman R. and Marijnissen J. (1996)., "Basic studies of electrohydrodynamic atomization using phase Doppler measurement technique", Part. Part. Syst. Charact. 13, 143-149.

Onofri F., Mignon H., Gouesbet G. and Gréhan G. (1995), "On the extension of phase Doppler Anemometry to the sizing of spherical multilayered particles and cylindrical particles", in Partec 95, Fourth International Congress on Optical Particle Sizing, (Nürnberg Messe GmbH, Nürnberg), pp. 275-284.

Onofri F., Blondel D., Gréhan G., Gouesbet G. (1996), "On the Optical Diagnosis and Sizing of Coated and Multilayered Particles with Phase Doppler Anemometry", Part. and Part. Syst. Charact. 13, 104-111.

Onofri F., Bergounoux L., Firpo J-L. and Mesguish-Ripault J. (1999), "Velocity, size and concentration measurements of optically inhomogeneous cylindrical and spherical particles", Appl. Opt. 38, 4681-4690.

Onofri F, Lenoble A., Radev S. (2002), "Superimposed Non Interfering Probes to extend the Phase Doppler Anemometry capabilities", accepted for publication in Appl. Opt. 41, N. 18.

Schaub S., Naqwi A. and Harding F.L. (1998), "Design of a phase/Doppler light-scattering system for measurement of small-diameter glass fibres during fibreglass manufacturing", Appl. Opt. 37, 573-585